Rainfall seasonality and timing: implications for cereal crop production in Ethiopia

Agricultural and Forest Meteorology 310 (2021) 108633

Contents lists available at ScienceDirect

Agricultural and Forest Meteorology

journal homepage: www.elsevier.com/locate/agrformet

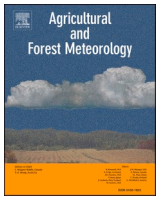

Rainfall seasonality and timing: implications for cereal crop production in Ethiopia

Mosisa Tujuba Wakjira [a,*], Nadav Peleg [b], Daniela Anghileri [c], Darcy Molnar [a], Tena Alamirew [d], Johan Six [e], Peter Molnar [a]

[a] Institute of Environmental Engineering, ETH Zurich, Stefano-Franscini-Platz 5, CH-8093 Zürich, Switzerland
[b] Institute of Earth Surface Dynamics, University of Lausanne, CH-1015 Lausanne, Switzerland
[c] Department of Geography and Environment, University of Southampton, University Road, SO17 1BJ Southampton, United Kingdom
[d] Ethiopian Institute of Water Resources, Addis Ababa University, PO.Box 1176, Addis Ababa, Ethiopia
[e] Department of Environmental Systems Science, ETH Zurich, Universitätstrasse 2, CH-8092 Zürich, Switzerland

ARTICLE INFO

Keywords:
Rainfall seasonality
Rainy season onset
Rainy season duration
Rainfed agriculture
Cereal crop production
Ethiopia

ABSTRACT

Rainfall seasonality and timing are key climatic features affecting crop yield in rainfed agriculture (RFA). We evaluated the dynamics of temporal rainfall attributes – the strength of seasonality, the date of onset, cessation, and duration of the rainy season – over RFA areas across Ethiopia for the period 1981-2010 and explored their impacts on cereal crop production (including maize, teff, sorghum, wheat, barley, millet, oats and rice) between 1995 and 2010. First, we quantified the rainfall seasonality using an entropy-based seasonality index, defined the onset and cessation dates of rainy seasons, computed the rainy season duration, and analyzed their interannual variability and trends. Second, we correlated de-trended total cereal production during the Meher (i.e., long rainy) season (April to September) with the anomalies of the temporal rainfall attributes, and we used a univariate linear regression model to estimate the influence of changes in these attributes on crop production. We show that RFA areas in northern Ethiopia are characterized by a highly seasonal and unimodal rainfall regime. The southern parts of the RFA areas are characterized by less seasonal rainfall of bimodal and erratic nature. Cereal crop production during the Meher season, especially in teff and maize-dominated regions, is found to be correlated to both the onset (median ρ=-0.32 and -0.37, respectively) and duration (ρ=0.34 and 0.19) of the rainy season in the unimodal rainfall regime, whereas it is correlated with the rainfall seasonality (ρ=0.21) in regions with a bimodal rainfall. We estimate that on average over RFA areas, a late-onset and shorter rainy season lead to ~1.5% and 1.1% crop production losses per pentad (5-day period), respectively.

1. Introduction

Rainfed agriculture (RFA) is based solely on green water (Falkenmark, 2006; Wani et al., 2009). The productivity of the rainfed farming system is determined by the temporal distribution of rainfall with respect to the cropping period in a given hydrological year (Guhathakurta and Saji, 2013; Hao et al., 2013) because this controls the amount of water stored in the soil that is available for biomass production. In RFA systems, farmers rely on their local knowledge of seasonal rainfall timing to match the cropping season with the time window over which rainfall provides adequate water to meet the water demand by the crop (Radeny et al., 2019). However, this is successful only when rainfall has a predictable temporal pattern, i.e. when the interannual variability at the start and end of the rainy season is low. The unpredictability of the timing of seasonal rainfall undermines productivity in smallholder RFA systems, particularly in sub-Saharan Africa, leading to food and livelihood crises (Guan et al., 2015; Torres et al., 2019). Thus, understanding the characteristics of seasonal rainfall concerning the growing season is of vital importance for planning and decision-making in rainfed farming systems (Guido et al., 2020; Victor et al., 1996).

In Ethiopia, about 95% of crop production is under smallholder rainfed practice (FAOSTAT, 2018) and largely takes place during the long rainy season called 'Meher' (April - September). Specifically, the June - September rainy months (locally known as 'Kiremt') account for 65 – 95% of the annual rainfall total over large parts of the country (Segele and Lamb, 2005). The arrival of Kiremt is preceded by the

* Corresponding author.
E-mail addresses: wakjira@ifu.baug.ethz.ch, mosisatujuba@gmail.com (M.T. Wakjira).

https://doi.org/10.1016/j.agrformet.2021.108633
Received 29 June 2021; Received in revised form 27 August 2021; Accepted 29 August 2021
Available online 8 September 2021

migration of the Intertropical Convergence Zone (ITCZ) (Hills, 1979) that brings the short rainy season (March - May), locally called 'Belg' (Korecha and Barnston, 2007). The Kiremt rainfall variability arises from its connection to the atmospheric circulation patterns at seasonal and interannual scales (Segele et al., 2009a) with local effects connected to topography (Dinku et al., 2008).

In light of its importance for agriculture, rainfall in Ethiopia has been extensively studied in relation to the mechanisms of atmospheric moisture transport to the region (Berhane and Zaitchik, 2014; Segele et al., 2009b; Viste and Sorteberg, 2013; Williams et al., 2012), teleconnections to large-scale oceanic and atmospheric phenomena (Camberlin, 1997; Degefu et al., 2017; Diro et al., 2011a, 2011b; Gleixner et al., 2017; Shanko and Camberlin, 1998), and the role of these teleconnections for rainfall prediction and forecasting (Gissila et al., 2004; Korecha and Barnston, 2007; MacLeod, 2018; Taye et al., 2021), as well as for seasonal and interannual variability and trends (Alhamshry et al., 2020; Cheung et al., 2008; Segele et al., 2015; Seleshi and Zanke, 2004). In addition, extreme climatic conditions that can have catastrophic effects on RFA systems, such as droughts, were also extensively studied (e.g., Funk et al., 2005; Philip et al., 2018; Temam et al., 2019; Viste et al., 2013).

The temporal rainfall attributes, such as the strength of seasonality in rainfall, the onset, cessation, and duration of the rainy season, are extremely relevant for decision-making in the RFA system. Rainfall seasonality is a measure of the spread in time of rainfall during the year (Walsh and Lawler, 1981). It has been studied in various parts of the globe to assess the responses of vegetation to the seasonal cycle of rainfall (e.g., Borchert, 1998; Dubois et al., 2014; Potter et al., 2005; Rohr et al., 2013; Souza et al., 2016; Suepa et al., 2016), and the impacts of seasonal rainfall variability on agriculture (e.g., Ayanlade et al., 2018; Guhathakurta and Saji, 2013; Sadiq, 2020). The onset and cessation of the rainy season have been studied in different parts of the world, such as in west Africa (e.g., Dodd and Jolliffe, 2001; Marteau et al., 2009; Omotosho et al., 2000), South America (González et al., 2007; Liebmann and Marengo, 2001; Marengo et al., 2001), and south and east Africa (Mugalavai et al., 2008; Raes et al., 2004). In Ethiopia, Segele and Lamb (2005) defined the Kiremt onset and cessation, and assessed its spatial variability across the country. Others explored the temporal properties of rainfall in Ethiopia and assessed the changes in dry spells, droughts and irrigation demand (e.g., Araya and Stroosnijder, 2011; Kebede et al., 2017; Seleshi and Camberlin, 2006). These studies are based on sparse station rainfall observation and thus, the findings are limited to specific sites, or spatially interpolated. Alternatively, high-quality gridded rainfall datasets (e.g., remote sensing and reanalysis products) can provide consistent results in regional studies.

One critical aspect that has not yet been studied in depth is the sensitivity of RFA to the temporal distribution of rainfall in Ethiopia. Thus, in this work, we quantify the temporal rainfall attributes using the Climate Hazards Group Infrared Precipitation with Station (CHIRPS) rainfall (Funk et al., 2015) and explore how they affect cereal crop production in the RFA areas of Ethiopia using national crop production data. We aim to answer three specific research questions: (a) how does the seasonality of rainfall vary in space across rainfed agricultural areas in Ethiopia? (b) do the temporal rainfall attributes describing seasonal rainfall exhibit trends in time, and (c) is crop production significantly related to these attributes and their changes?

2. Study area and data

The study area covers the entire arable RFA area (Fig. 1a) of Ethiopia (cropland covers 33% of the RFA area, elevation ranges between 340 and 4500 m.a.s.l) that was delineated by Kassawmar et al. (2019) by reclassifying the biophysical factors (rainfall, temperature, altitude and slope) and combining them with crop production data. The size of the study area is about 667,000 km^2, which is 59% of the total landmass of Ethiopia and is inhabited by more than 90% of the total population (CSA, 2007). The climate varies from arid on the eastside peripheral areas, where the mean annual rainfall is as low as 270 mm, to humid in the western and southwestern areas with mean annual rainfall up to 2100 mm (Fig. 1b). Mean annual temperature (Fig. 1c) generally increases from the central and northern highlands towards the western and northwestern lowlands and from eastern highlands to the southeastern lowlands, separated by the southwest-northeast oriented warm Rift Valley corridor.

Daily rainfall data at a spatial resolution of 0.05° x 0.05° for the region were obtained from the CHIRPS dataset (Funk et al., 2015) for the period 1981-2010. CHIRPS rainfall was evaluated in past studies across East Africa (Dinku et al., 2018; Gebrechorkos et al., 2018) and for specific watersheds in Ethiopia (Bayissa et al., 2017; Gebremicael et al., 2019; Musie et al., 2019), where it outperformed other gridded global rainfall datasets. CHIRPS data were also compared with the rainfall at 65 ground stations in the study area and it was demonstrated that they sufficiently match at pentadal (5-day accumulation) scale as shown in Fig. 2. The comparison of CHIRPS and stations shows little bias and a high correlation (ρ=0.86), with expected spread due to point versus grid rainfall and estimation errors, and larger discrepancies at stations

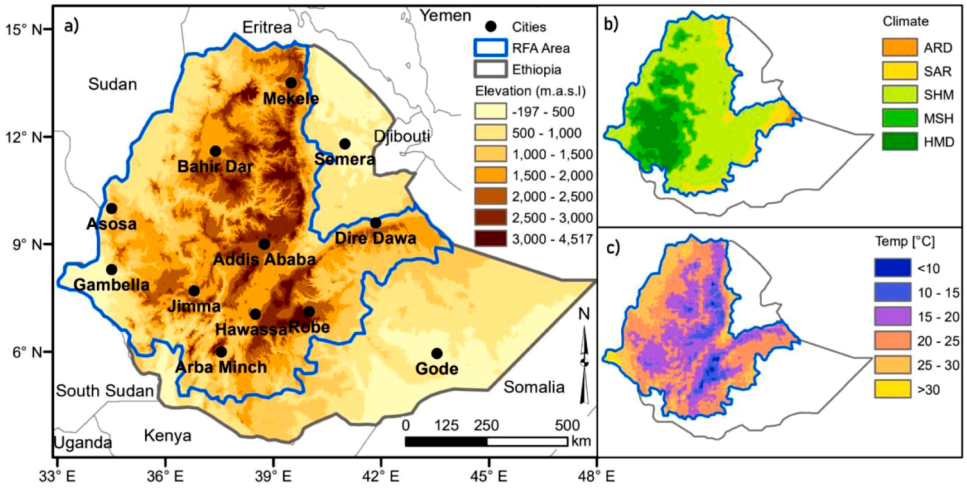

Fig. 1. (a) Map of Ethiopia and the RFA area (blue outline (Kassawmar et al., 2019)). (b) Climatic zones based on the FAO classification (FAO, 1986) of mean annual CHIRPS rainfall (1981-2010). ARD = arid, SAR = semi-arid, SHM = sub-humid, MSH = moist sub-humid, HMD = humid. (c) Mean annual temperature (1981-2010) based on the CFSR data (Saha et al., 2010).

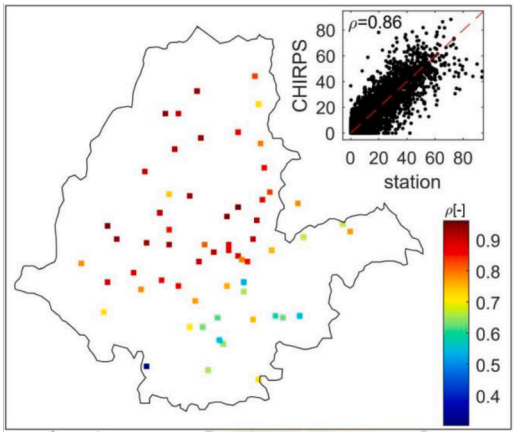

Fig. 2. Correlation coefficient (ρ) of CHIRPS grids versus ground station pentadal (5-day accumulation) rainfall averaged for all 73 pentads of every calendar year over the period 1998-2007 at 65 sites across the study area. The inset shows the scatterplot of the gridded and station pentad rainfall with 65 × 73 data points. Pentads with zero mean rainfall are included in the analysis.

southeast of the rift valley. This is also observed in other gridded rainfall datasets (Dinku et al., 2018).

The CHIRPS gridded data allows the classification of the RFA area into several rainfall regimes (Fig. 3) based on the seasonal rainfall pattern (unimodal or bimodal) and the FAO classification of climatic zones (FAO, 1986). Regimes 1-3 (R1-R3) are characterized by a unimodal rainfall pattern while regimes 5-6 (R5-R6) have a bimodal pattern, and regime 4 (R4) is considered as transitional (unimodal to bimodal).

We obtained the annual Meher crop production data from the annual statistical bulletin (available at https://www.statsethiopia.gov.et/our-survey-reports/) of the Central Statistical Agency (CSA) of Ethiopia. The CSA conducts an annual post-harvest agricultural survey that involves more than 32,000 agricultural households across the country to collect crop production data of all crop types that are produced in the country, and summarizes the crop statistics at regional and zonal (sub-regional administrative unit) scales (CSA, 2010). Cereals (maize, teff, sorghum, wheat, barley, millet, oats and rice) are staple crops and account for about 87% of the total grain production in the country.

3. Methods

In the analyses of temporal rainfall patterns and their effects on crop production, we first quantified the strength of rainfall seasonality using the method introduced by Feng et al. (2013). The approach is based on the concept of entropy (Cover and Thomas, 2005) and defines a seasonality index based on two rainfall properties: annual rainfall and a measure of monthly rainfall variability labeled as relative entropy. This approach enables a spatial mapping of rainfall seasonality with respect to a predefined reference location (e.g., location with maximum rainfall). Next, we defined the rainfall timing attributes, i.e. the onset and cessation of the rainy season, from cumulative rainfall anomaly curves (Dunning et al., 2016; Liebmann et al., 2012; Liebmann and Marengo, 2001). This well-established objective approach is particularly suitable for analysis of rainfall timing at regional scales (González et al., 2007; Hampf et al., 2020; Jiang et al., 2019; MacLeod, 2018; Zhang et al., 2018). We then analyzed the variability and trends in all the temporal rainfall attributes. Lastly, we examined the statistical relationships between these attributes and total cereal production using parametric Pearson correlation and linear regression. Details of the methods are presented in the following sections.

3.1. Determination of rainfall seasonality

We examined the rainfall seasonality over the RFA area at grid-scale for the period 1981-2010 based on the method proposed by Feng et al. (2013). They defined two rainfall seasonality metrics: the Relative

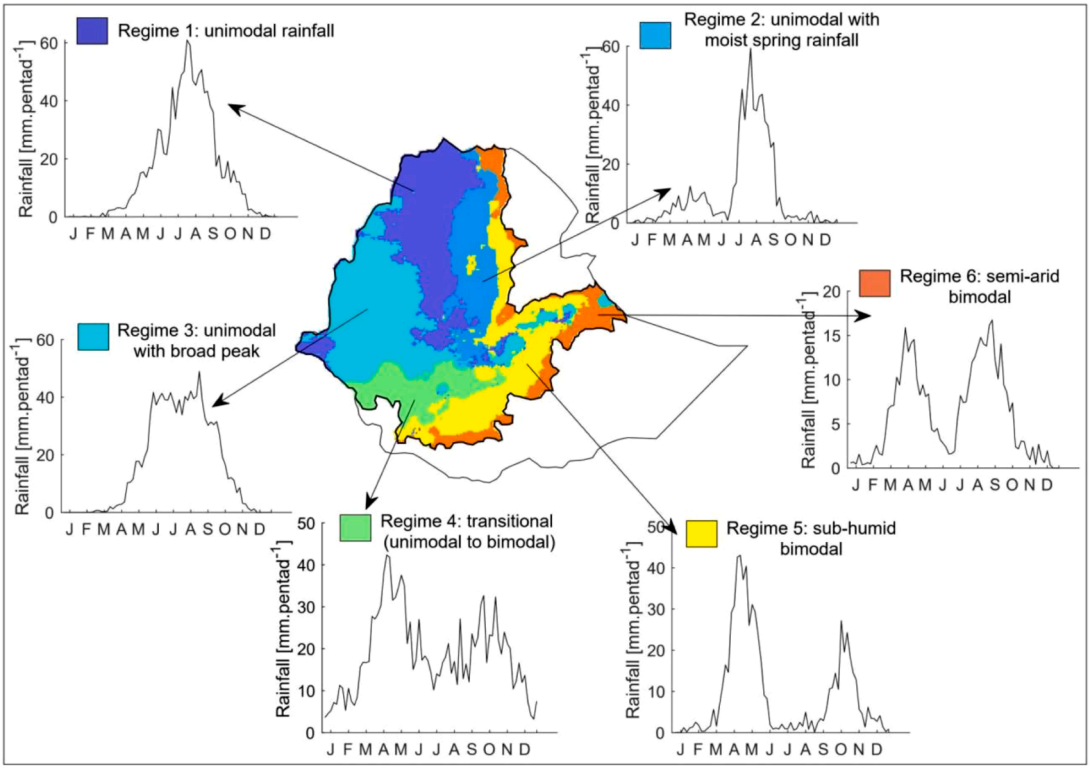

Fig. 3. Rainfall regimes of the RFA area of Ethiopia as classified based on CHIRPS rainfall climatology of the period 1981-2010. Insets show examples of pentad (5-day) mean rainfall at arbitrary locations for each regime.

Entropy (RE) and the Dimensionless Seasonality Index (DSI). The relative entropy for a given calendar year k, RE_k, where in our analysis $k \in [1,30]$, is a measure of how different the actual rainfall distribution is from the uniform distribution. It is computed for each grid point as $RE_k = \sum_{m=1}^{12} p_{k,m} \log_2(p_{k,m}/q_m)$, where $p_{k,m} = r_{k,m}/R_k$ is the actual monthly rainfall probability ($r_{k,m}$ is the rainfall in the month m of year k, and R_k is annual total rainfall of year k), and $q_m = 1/12$ is the theoretical monthly rainfall probability of a non-seasonal (uniform) rainfall regime. Theoretically, RE_k is zero when R_k is equally distributed over all months of the year (i.e., when $p_{k,m} = q_m = 1/12$ for $m \in [1,12]$) and attains a maximum value when R_k is concentrated in a single month. The dimensionless seasonality index for a given calendar year k is then computed as $DSI_k = (R_k/R_{max})RE_k$, where the scaling factor R_{max} is the maximum annual rainfall in the dataset, which in our study area is 2678 mm. A maximum value of DSI_k corresponds to a rainfall regime with R_k concentrated within a single month (maximum RE_k), whereas a zero value of DSI_k is due to either a completely dry year (R_k=0) or a uniformly distributed R_k (RE_k=0).

3.2. Defining the onset and cessation of the rainy season

We defined the timing of the rainy season at grid-scale by the dates of the onset and cessation of rainfall based on pentad (5-day) rainfall totals. In the first step, we computed for each grid cell the climatological mean rainfall P_c of each pentad i of the calendar year as: $P_{c,i} = (\sum_{k=1}^{30} P_{i,k})/30$, ($i \in [1,73]$, i.e., 73 pentads in a calendar year), as well as the long-term pentadal mean $\overline{P} = (\sum_{i=1}^{73} P_{c,i})/73$ from the 30-year rainfall record. In the second step, we calculated the climatological cumulative rainfall anomaly, $C_c(p) = \sum_{i=1}^{p} (P_{c,i} - \overline{P})$ with $p \in [1,73]$.

We used the same expression to compute the cumulative rainfall anomaly for every calendar year k as a cumulative sum of the difference between the pentadal rainfall of that year and $\overline{P}$. In Fig. 4 we show an example of cumulative anomaly curves constructed from a bimodal rainfall regime (climatological and an example of a single year). The long-term pentadal mean $\overline{P}$ at any grid cell is the threshold that determines the onset and cessation pentad of the year, i.e., when $P_{c,i}$ is less than $\overline{P}$, the cumulative anomaly curve has a negative slope and vice versa. The onset pentad is defined as the pentad after which the slope of the curve changes from a persistent negative to a persistent positive (the green dots in Fig. 4b). Likewise, the cessation pentad is the pentad after which the slope changes from positive to negative (the red dots in Fig. 4b). The duration of the rainy season is defined as the difference between the date of the cessation and onset pentad.

We located the onset and cessation pentads by identifying the minimum and maximum of the anomaly curve for both unimodal (one onset and cessation) and bimodal (two onsets and cessations) regimes. To mask out local minima and maxima along the curve (e.g. blue curve in Fig. 4b), we smoothed the curve (not shown in Fig. 4b) using the non-parametric LOESS smoother (Cleveland, 1979). Locating the onset and cessation pentads in all rainfall regimes except Regime 4 is straightforward. Regime 4 is a transitional regime (see Fig. 3) where the rainfall pattern lacks interannual consistency and the rainfall cumulative anomaly curve has multiple peaks even after smoothing, which complicates the location of the cessation pentad. In this case, we assumed the last peak of the curve as the cessation pentad. Finally, we examined the long-term trends of the temporal rainfall attributes (seasonality, onset, cessation and duration) from the annual estimates. For this purpose, we applied the non-parametric Mann-Kendall test (Kendall, 1975; Mann, 1945) to detect trends and estimate their statistical significance, and the Sen slope estimator (Sen, 1968) to estimate the magnitude of the trends.

3.3. Correlation between temporal rainfall attributes and crop production

The temporal rainfall attributes obtained above were related to the annual Total Cereal Production (TCP) during the Meher (April to September) season in 45 zones (Fig. 5a) across the RFA area. To match the spatial resolution of the TCP dataset with that of the CHIRPS rainfall dataset, we disaggregated the zonal TCP in space down to the CHIRPS grid (5 km x 5 km) using the Cropland Cover Fraction (CCF) map obtained from the Copernicus Global Land Services (Buchhorn et al., 2020). The annual CCF maps are available at 100 m x 100 m resolution for the period 2015-2019. We averaged the CCF during the period 2017-2019 (2015-2016 were excluded as these were drought years) and aggregated the data to a 5 km x 5 km grid (Fig. 5b), from which we computed the cropland area in km^2 in every grid cell (i,j) as: $A_{(i,j)} = 25(CCF_{(i,j)}/100)$. The TCP of a grid cell (Fig. 5c) that is located in zone $n \in [1, 45]$ in the calendar year $k \in [1, 16]$ was then calculated as: ${}^{n,k}TCP_{i,j} = {}^{n,k}TCP({}^{n}A_{i,j} / \sum({}^{n}A_{i,j}))$, where the sum goes over all cells in zone n. The temporal ranges of CCF (2017-2019) and TCP (1995-2010) do not overlap and this could introduce uncertainties in the disaggregation if cropland cover changes significantly over time. However, these changes can be considered slow as they involve both degradation (abandoned cropland) and expansion (Kassawmar et al., 2018) and thus, the effects of these changes compensate when the CCF data is aggregated from the fine to coarse resolution. The disaggregation process is illustrated in Fig. 5.

We observed a significant upward trend (on average at 6% yr^{-1}) in the TCP dataset over the entire RFA area, which is primarily attributed to non-climatic factors, including improvements in agricultural inputs like access to fertilizer, seed, cultivation and harvesting technologies (Gebeyehu, 2016; Shikur, 2020), and some expansion of the cultivated areas (Taffesse et al., 2012). We de-trended the TCP data to remove these effects, so that interannual variability in TCP can be more clearly related to the temporal rainfall attributes only (Kukal and Irmak, 2018). We then computed the Pearson correlation between the anomalies in the temporal rainfall attributes and the de-trended TCP, after inspecting the linearity of the predictor-response relationship, normality of the residuals, and independence of the data. To understand the relationship

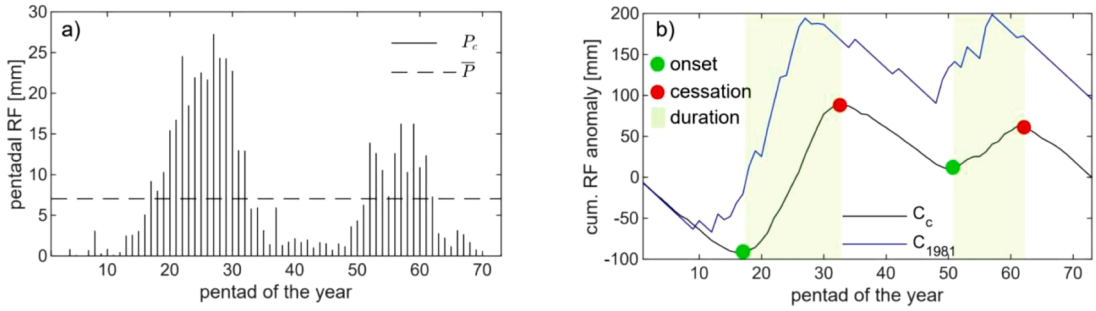

Fig. 4. Example of cumulative anomaly curves for the bimodal rainfall regime: (a) Climatological pentadal rainfall at grid cell 8.07°N and 41.82°E and mean P. (b) The corresponding climatological cumulative anomaly curve (black) and cumulative anomaly curve for the year 1981 (blue). The onset (green dots) and cessation (red dots) pentads define the climatology of the two rainy seasons (light green areas) and their durations.

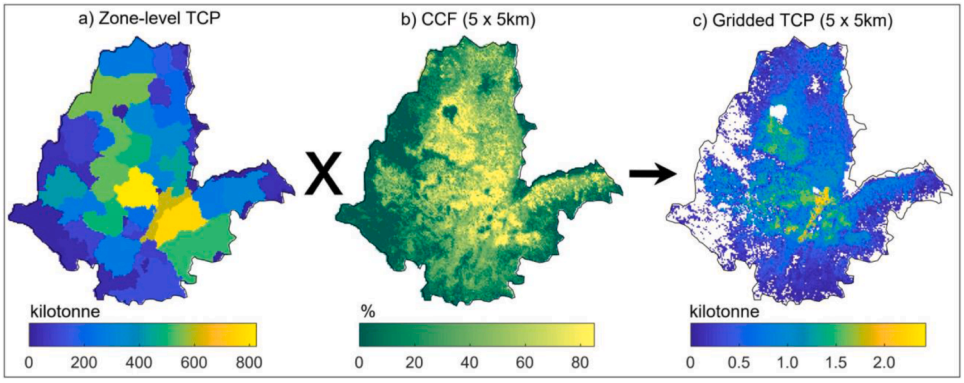

Fig. 5. Spatial disaggregation of crop data: (a) zonal Meher total cereal production (averaged over 1995-2010), (b) cropland cover fraction (CCF) aggregated from 100 m x 100 m to 5 km x 5 km resolution, and (c) disaggregated gridded TCP.

between specific cereal crop production and changes in the temporal rainfall attributes, we separately analyzed the correlation at 25 grid cells across the RFA area where each of the four major cereal crops (maize, teff, sorghum and wheat) dominates the total cereal production as mapped in the Atlas of the Ethiopian Rural Socioeconomy (IFPRI and CSA, 2006). Lastly, we estimated the magnitude of the effects of changes in the temporal rainfall attributes on crop production by fitting a univariate linear regression model with anomalies in the attributes as a predictor and the de-trended TCP as a response variable.

4. Results and discussion

4.1. Rainfall seasonality and its dynamics

High rainfall seasonality is observed in the northern RFA area, particularly in regimes R1, R2 and parts of R3, where RF and RE are simultaneously intermediate to high (Fig. 6). However, the pattern of DSI largely follows the pattern of RF indicating that the strength of rainfall seasonality in these regions is mainly controlled by the annual rainfall amount. In contrast, the southern part of the RFA area (R4-R6) is characterized by low rainfall seasonality. The pattern of DSI predominantly follows the pattern of RE and thus, the strength of rainfall seasonality in these areas is mainly controlled by the monthly distribution of rainfall. For example, the southwestern area (R4 and lower part of R3) where DSI is extremely low is characterized by short dry months (low RE) and medium to high RF (sub-humid to humid climate), although the effect of RF on seasonality is not visible in this region (Fig. 6).

The relevance of rainfall for rainfed crop production is determined by its temporal distribution in reference to the cropping season (Mutsaers, 1979; Yengoh et al., 2010). In this regard, the observed low seasonality in R4 and parts of R3 in the southwest of the RFA area is desirable because it allows effective exploitation of the high annual rainfall for double-cropping, while the temporal distribution of rainfall in the wet regions such as the middle and upper parts of R3 (Fig. 6a, c) tends to limit double-cropping due to high seasonality, despite high annual rainfall. Conversely, low seasonality is problematic in arid and semi-arid climates such as R5 and R6 because low rainfall over an extended period can constrain the relevance of the rainy season for crop production. For example, the bimodal regime (low seasonality) in the eastern semi-arid parts of the RFA area where the annual rainfall is less than 600 mm is less efficient for crop production because the annual rainfall is partitioned into two distinct seasons but with lower rainfall amounts.

Considerable interannual variability in rainfall seasonality is observed over large parts of the RFA area. The northeastern semi-arid and sub-humid areas that include parts of R2 and R5 (Fig. 7a), show an average coefficient of variation (CV) of 0.34, which is due to variability in RE (Fig. 7b) intensified by the small variability in the RF (Fig. 7c). Similarly, the natural variability in the seasonality of rainfall is high in R4 with a regional average CV of 0.38, and this variability is purely attributed to the variability in RE. The western and northwestern side (parts of R1 and R3) of the RFA area is characterized by stable seasonality patterns, whereas R5, R6 and parts of R2 and R3 have moderate variability in rainfall seasonality.

Parts of the RFA area experienced a significant increase in seasonality (DSI, Fig. 7d) in the period 1981-2010. Specifically, R2 and R5 (area marked by the red rectangle) are found to have an increase in the seasonality of 2% yr^{-1} on average, as a result of the expanding number of dry months (increase in RE, Fig. 7e) and an increase in annual rainfall (Fig. 7f). Similar trends are also observed in parts of R4 and R5 in the

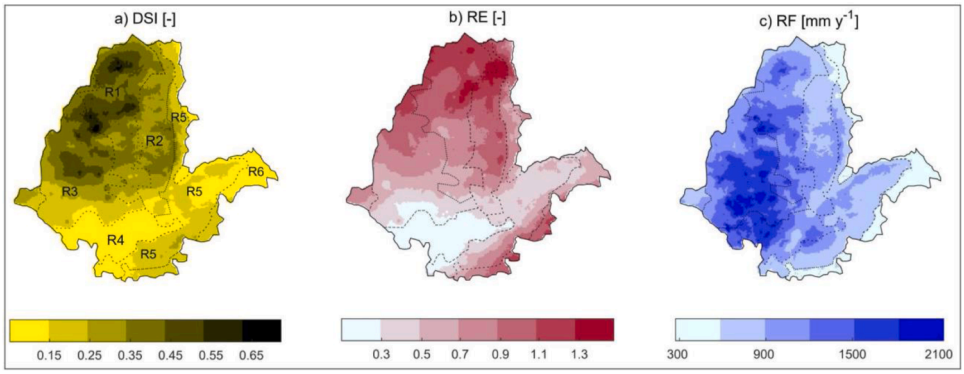

Fig. 6. Maps of the rainfall seasonality metrics in the RFA area of Ethiopia: (a) mean dimensionless seasonality index (DSI), (b) mean relative entropy (RE), and (c) mean annual rainfall (RF), computed for the period 1981-2010. The layer with dotted boundaries shows the rainfall regimes R1-R6 (see Fig. 3 for their detailed representation).

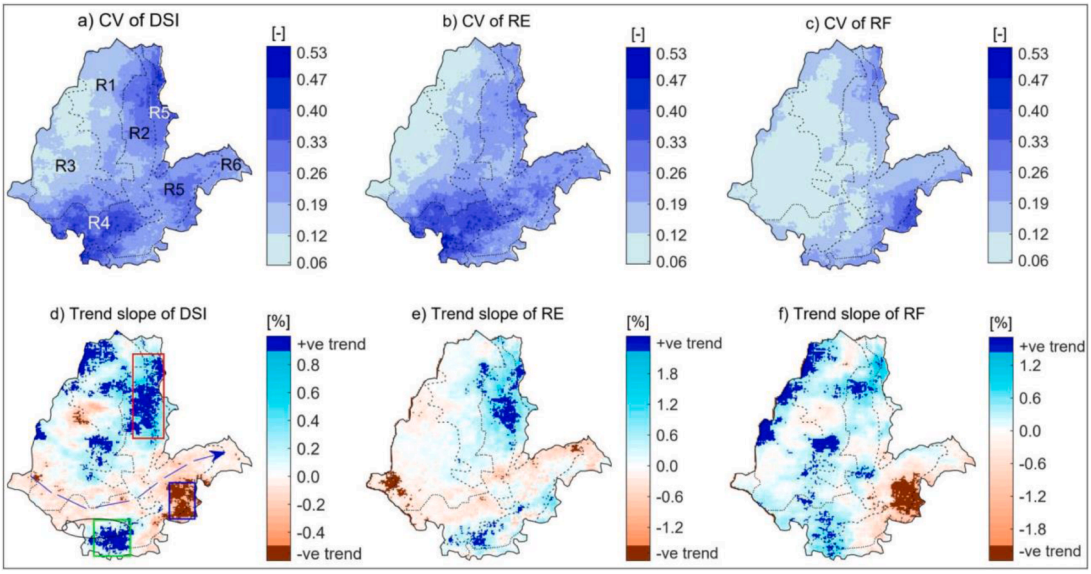

Fig. 7. Interannual variability and trends in rainfall seasonality metrics: (a-c) Coefficient of variation of the dimensionless seasonality index DSI, relative entropy RE, and annual rainfall RF. (d-f) Trend slope in %/yr (shown by the light blue and light brown color schemes) and statistically significant trends ($\alpha = 0.05$) in the metrics in the period 1981-2010; dark blue color - positive trend, and dark brown - negative trend. The dotted lines represent the rainfall regimes (R1-R6).

southern sub-humid area (the green rectangle). Furthermore, the increasing tendency of seasonality over the northwestern lowlands (R1) is exclusively attributed to the positive trend in annual rainfall. On the contrary, seasonality tends to significantly decrease across the belt of the RFA area (Fig. 7d, blue dashed arrow) following the decreasing tendency of RE. A significant decrease in DSI is observed over the dry southeastern part (blue rectangle) of the RFA area because of the decreasing trend in annual rainfall (Fig. 7f).

The observed changes of rainfall seasonality in time are related to drought occurrences over the RFA area. Viste et al. (2013) investigated droughts in Ethiopia over 40 years, including the period considered in this analysis. They found a frequent Belg (March to May) drought with a 36% probability of occurrence over the northeastern semi-arid and sub-humid areas (parts of R2 and R5), and a frequent Kiremt drought with a 42% probability of occurrence over the southern humid and sub-humid areas (parts of R4 and R5). Given that the increase in seasonality in these regions is attributed to the combined effects of the simultaneous increase in the annual rainfall and the number of dry months, it can be concluded that an increase in seasonality expected when the increase in rainfall occurs during the long rainy season (Kiremt in the northeast and Belg in the south), and a decrease in rainfall occurs during the short rainy season (Belg in the northeast and end of Kiremt in the south). Therefore, the observed increase in the rainfall seasonality is strongly related to rainfall deficit during Belg in the northeast, and during Kiremt over the southern parts of the RFA areas. On the contrary, a decrease in seasonality can occur due to a rainfall deficit mainly during the Kiremt season. The Kiremt rainfall deficit over Ethiopia is largely related to El Niño conditions (e.g., Diro et al., 2011b; Gleixner et al., 2017; Korecha and Barnston, 2007; Segele and Lamb, 2005) and thus, one can expect a systematic relation between El Niño conditions and rainfall seasonality. From a simple comparison of the temporal patterns of the mean annual NINO3.4 SST index and the median annual DSI anomalies over the entire RFA grids, we found that rainfall seasonality over the RFA areas is negatively correlated (ρ=-0.66) with the Equatorial Pacific sea surface temperature. This implies that a decrease in rainfall seasonality is expected under El Niño conditions.

4.2. Rainfall onset, cessation and their dynamics

The climatological onset of the rainy season ranges from early March to early September (Fig. 8a). The earlier onset is in R4 in the south and southwest (dark blue areas) and rapidly propagates to later dates in R3. The subsequent propagation of the onset follows northwestward from R3 and advances slowly in the northeast direction across R1 and R2 until it arrives at R5 in the northeastern and eastern peripheral areas (yellow areas) in late June/early July. The later onset in the southern and southeastern areas (light brown areas in R5 and R6) is related to the onset of the short rainy season in autumn that ends in late November.

The climatological cessation of rainfall (Fig. 8b) generally follows the reverse direction of the onset with early cessation during late September in the northeastern semi-arid areas (dark green color). It first progresses southward along R2 and R5 to the central part over about two weeks and then propagates slowly southwestward until the end of October, followed by the later episode of cessation of the short autumn rainfall at the end of November. As a result, the duration of the main rainy season (Fig. 8c) over the RFA area generally decreases from R4 in the southwest (250 days) across R3 towards east and northeast where the duration is as short as 80 days. The total rainfall enclosed by the defined onset and cessation dates accounts on average for about 79% of the annual rainfall across the RFA area (Fig. 8d).

Comparable findings were documented by Segele and Lamb (2005) who followed a threshold-based approach using rainfall data from 121 ground weather stations to define the onset and cessation of Kiremt over a similar study area. A significant discrepancy with this study lies in the long rainy season in R5 along the eastern highlands (the dark blue strip in Fig. 8a). In fact, the rainfall pattern over this region has a bimodal tendency, but without distinct dry periods between the peaks. With the approach we used for the definition of the onset and cessation, the rainfall peaks are not detectable on the cumulative anomaly curve unless the subsequent pentads are persistently drier than the long-term pentadal mean, which is not the case in this region.

The progression of rainfall timing in space is associated with the atmospheric flow pattern over the East African region. The earlier onset in March across the southwest–east strip (see Fig. 8a) is triggered by the northward migration of the ITCZ following the warming of the northern hemisphere (Segele and Lamb, 2005). This is followed by a continuous influx of moist air masses mainly from the Gulf of Guinea (Diro et al., 2011a; Segele et al., 2009b; Viste and Sorteberg, 2013) that flow northeastward, i.e. the same orientation of the onset progression, supplying moisture to the region during the entire Kiremt. The moisture flux

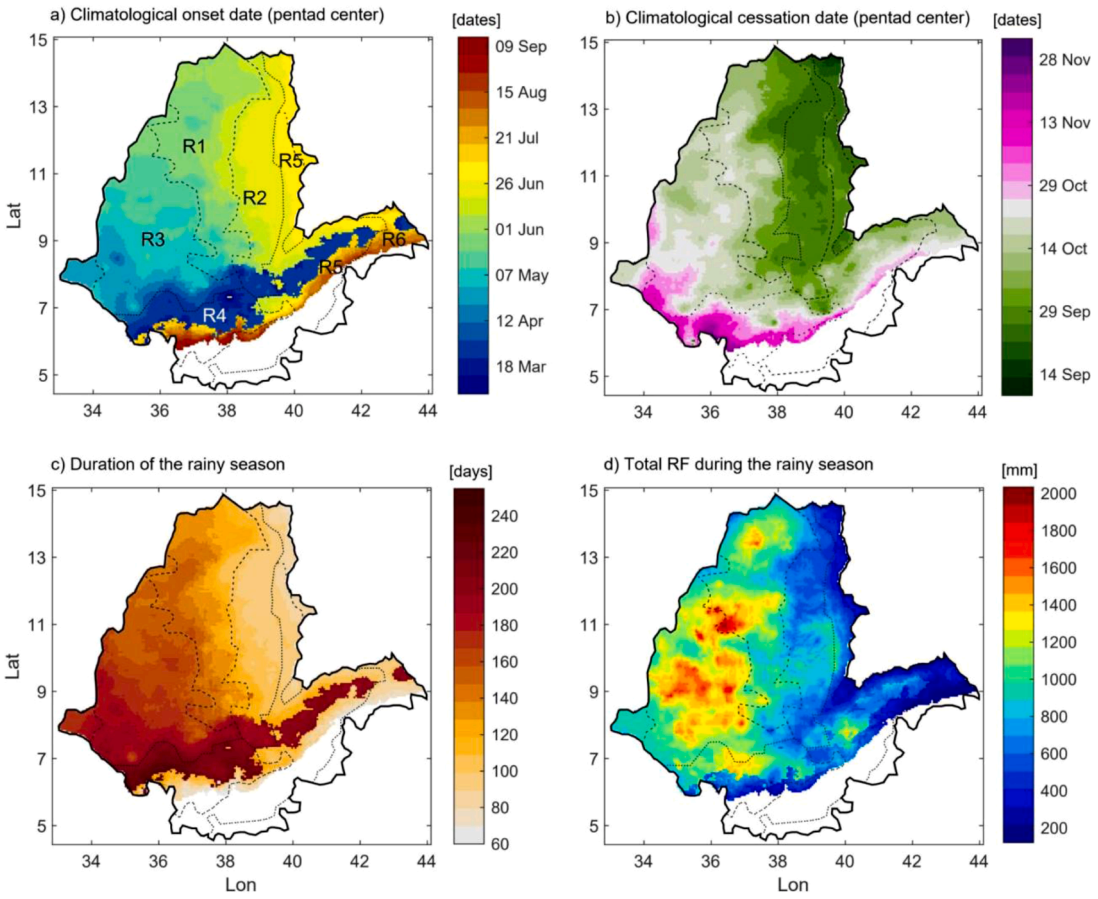

Fig. 8. Climatology of the average onset (a) and cessation (b) of the rainy season given by the mean date, length of the rainy season (c), and total rainfall during the main rainy season (d) for the period 1981-2010. The blank part of the maps represents areas where the Kiremt rainfall is <25% of the annual rainfall and the duration of the rainy season is <60 days. The dotted lines represent the rainfall regimes (R1-R6).

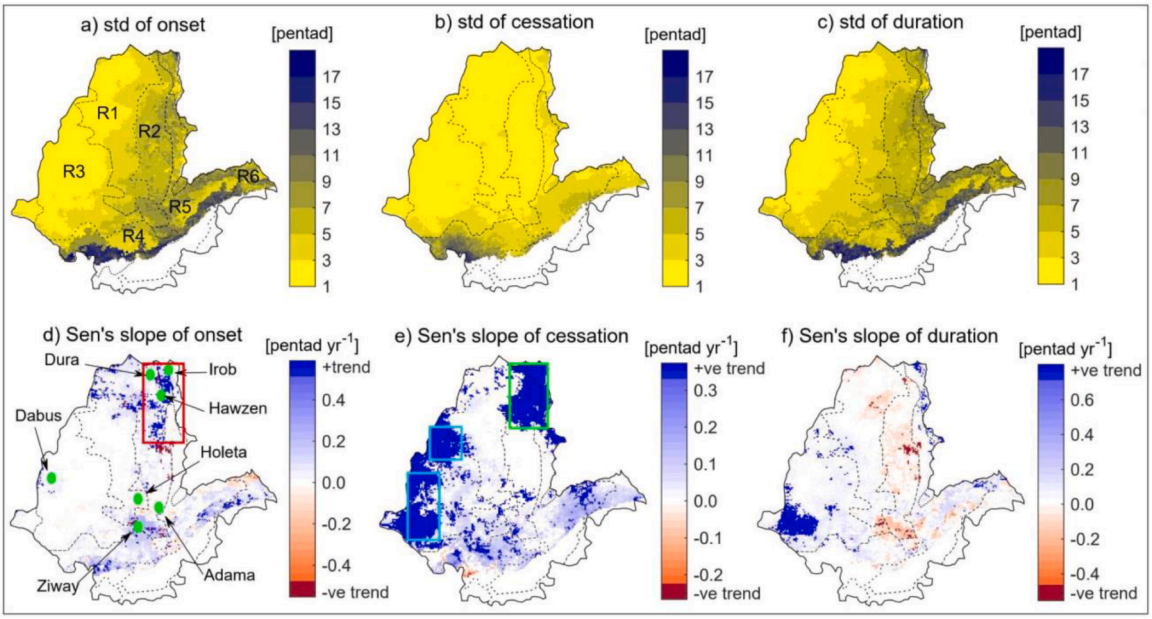

Fig. 9. Interannual variability and trends in rainfall timing: standard deviation of onset (a), cessation (b) and the duration of the rainy season (c) in pentads for the period 1981-2010; Sen's slope and trends in the onset (d), cessation (e) and length of the rainy season (f). The dark blue and brown colors in panels d-f represent statistically significant positive and negative trends respectively. The green dots in (d) are the site locations of recent studies (Asrat and Simane, 2018; Habtemariam et al., 2016; Hundera et al., 2019; Kahsay et al., 2019; Tesfahunegn et al., 2016) where farmers' perception of local climate changes were documented. The dotted lines represent the rainfall regimes (R1-R6).

into the region is controlled by the equatorial Pacific sea surface temperature anomalies (Diro et al., 2011b; Gleixner et al., 2017; Segele and Lamb, 2005), with a retarding effect during El Niño conditions. As a result, about 54% of the late-onset during the period 1981-2010 occurred under El Niño conditions. The southwestward retreat of Kiremt is triggered by the weakening of the westerly winds and the southward movement of the ITCZ (Dunning et al., 2016; Segele and Lamb, 2005). The latest cessation of the rainy season during late November over the southwestern region (pink areas in Fig. 8b) is related to the persistence of the ITCZ in the south.

Analyzing annual data, we observed high interannual variability in the onset (median standard deviation of 4.13 pentads, Fig. 9a) and in the duration (median standard deviation of 3.67 pentads, Fig. 9c) of the rainy season, which are also well correlated (Pearson's ρ=0.96). The patterns of variability in onset and duration change in the opposite direction with the pattern of rainfall seasonality (Section 4.1) with ρ=-0.6. In other words, the onset date and duration of the rainy season is highly variable in bimodal rainfall regimes (R5 and R6, parts of R2 and R4). Furthermore, we found that the variability of rainy season duration explains a substantial portion (ρ=0.66) of the variability in DSI.

The cessation of the rainy season is more stable (median standard deviation of 1.91 pentads, Fig. 9b) compared to the onset. This difference can be partially attributed to the topography of the RFA area that influences the air mass flow (Dinku et al., 2008; Gissila et al., 2004) during the onset of the rainy season. The extreme variability along the southern and southeastern periphery (dark grey areas in Fig. 9a-c) is related to instability of the onset in the strongly erratic and unpredictable rainfall areas.

Our findings on spatial variability are not in full agreement with the findings of Segele and Lamb (2005) in terms of the pattern and magnitude of the variability in the onset of the rainy season. They found a decrease in the standard deviation of the onset from northeast to southwest regions with a lower average magnitude of approximately 3 pentads. However, the findings on variability in the cessation date agree to a larger degree, both in terms of pattern and magnitude. The discrepancy may be due to the methods used in defining the rainfall onset, as well as the differences in interpolated ground station used by Segele and Lamb (2005) versus the CHIRPS rainfall data that we used.

Regarding the long-term changes in the rainfall timing attributes over the period 1981-2010, we found a significant trend of late-cessation of the rainy season over large parts of the northeastern semi-arid areas (green rectangle, Fig. 9e), western sub-humid lowlands in R3 (blue rectangles), and certain parts in the central and eastern parts of the RFA area. The trend towards late-cessation in the northeast (R2 and R5) coincides with parts of the areas where a significant increase in seasonality was detected (see Section 4.1). Additionally, few areas in this particular region (red rectangle, Fig. 9d) have undergone significant changes toward late-onset and shortening of the duration (Fig. 9f). These three signals of change (late-onset, late-cessation and shortened duration) complement our earlier finding that the increase in seasonality in this region is associated with the recurrent failure of the Belg rainfall (Viste et al., 2013) and increased and (slightly shifted and shortened) Kiremt rainfall.

The changes observed in the onset and duration of the rainy seasons are in agreement with the farmers' perception, particularly in the hotspot regions, such as the northeastern semi-arid areas in R2. In recent assessments of farmers' perception of local climate change at various sites (the green dots in Fig. 9d), e.g., at Dura (Tesfahunegn et al., 2016), Irob and Hawzen (Kahsay et al., 2019), and at Ziway (Habtemariam et al., 2016), over 81% of the respondents reported a perceived late-onset of the rainy season. Asrat and Simane (2018) show farmers' perception in the Dabus area of shortening duration of the rainy season (in agreement with our findings) and late-onset (contradicting our findings). At Holeta (Habtemariam et al., 2016) and Adama (Hundera et al., 2019), farmers perceive late-onset, while we found a tendency of early-onset in these areas. Although the periods considered in these studies do not perfectly match with the period covered in our analysis, the data indicate that the impacts of the changes detected in climatic indicators are perceived at the farm level.

The trends in the temporal rainfall attributes, i.e., seasonality (section 4.1), onset, cessation and duration of the rainy season during the recent climate normal (1981-2010) is an indication of the impact of climate change on the temporal distribution of rainfall in the study region. Given the importance of the temporal attributes of rainfall for rainfed farming systems, these changes can have major impacts on crop production as discussed in section 4.3. It is important also to note that changes in the temporal rainfall attributes can intensify under future climate (Dunning et al., 2018; Gaetani et al., 2020; Pascale et al., 2016), which may have additional implications on the RFA systems.

4.3. Implications of rainfall seasonality and timing for crop production

Among the four temporal rainfall attributes (seasonality, onset, cessation, and duration), the onset of the rainy season strongly determines the Meher TCP (Fig. 10a). Late-onset (positive onset anomaly) is accompanied by a decrease in TCP and vice versa. The effect of cessation on TCP (Fig. 10b) is spatially inconsistent, although positive or negative correlations are detected in specific areas. TCP is positively correlated with the duration of the rainy season in many areas (Fig. 10c). We also observed a weak positive correlation between TCP and seasonality (median ρ=0.03 considering all regions, Fig. 10d).

The influence of the rainfall onset on TCP is more pronounced in unimodal regimes, R1 and R3 (ρ=-0.40 and -0.38, respectively). The negative correlation in R1 is associated with high rainfall seasonality where the rainy season is confined between June and September. TCP in both R1 and R3 are positively correlated with the duration of the rainy season (ρ=0.28 and 0.19, respectively). However, the effect of seasonality in these regimes is small and tends to be negative. Compared to R1 and R3, the correlation between TCP and onset is lower in R2 (ρ=-0.22), where Kiremt is preceded by the short Belg rainfall. This may be related to the soil moisture memory from the Belg season that can reduce crop failure during germination before the Kiremt onset. The positive correlation (ρ=0.19) with the duration is not manifested in DSI in R2.

TCP is weakly correlated with the rainfall onset and duration of the rainy season in R4, R5 and R6 where rainfall is less seasonal. For example, in R4, where there are only a few dry months, the most important rainfall timing attribute is the rainfall cessation (ρ=0.17). This is because Meher is the second production season after the main Belg production (CSA, 2016), and thus late cessation is an advantage. In the bimodal regimes R5 and R6, we found that seasonality is the most determinant factor for TCP because it is positively correlated with DSI (ρ=0.2, for both regimes), while the correlation with the other attributes is relatively weak. As discussed in section 4.1, overextended rainfall (less seasonal) in regions with low rainfall such as R5 and R6 is not reliable for crop production during the growing season. In line with the present findings, Tesfaye and Seifu (2016) reported that the failure of rainfall to support crop production is one of the effects of climate variability and change perceived by farmers over the previous 10-15 years at Babile, Fedis and Kersa sites in the eastern part of the RFA area (see the red dots in Fig. 10d).

Next, we explored if the relationships between TCP and the temporal rainfall attributes discussed above when considering the total cereal production is different for specific crops. We found that the general pattern of the correlation for specific crops follows the same direction as that of the total cereal production, but the strength of the correlation changes between crops (Fig. 11). Rainfall onset has a greater impact on maize and teff (ρ=-0.37 and -0.32, respectively) compared to sorghum and wheat (ρ=-0.19 for both). The influence of the duration of the rainy season (Fig. 11c) is highest for teff (ρ=0.34) compared to the other crops. A weak correlation is observed for DSI (Fig. 11d), with a negative tendency for teff and maize versus a positive tendency for sorghum and no correlation for wheat.

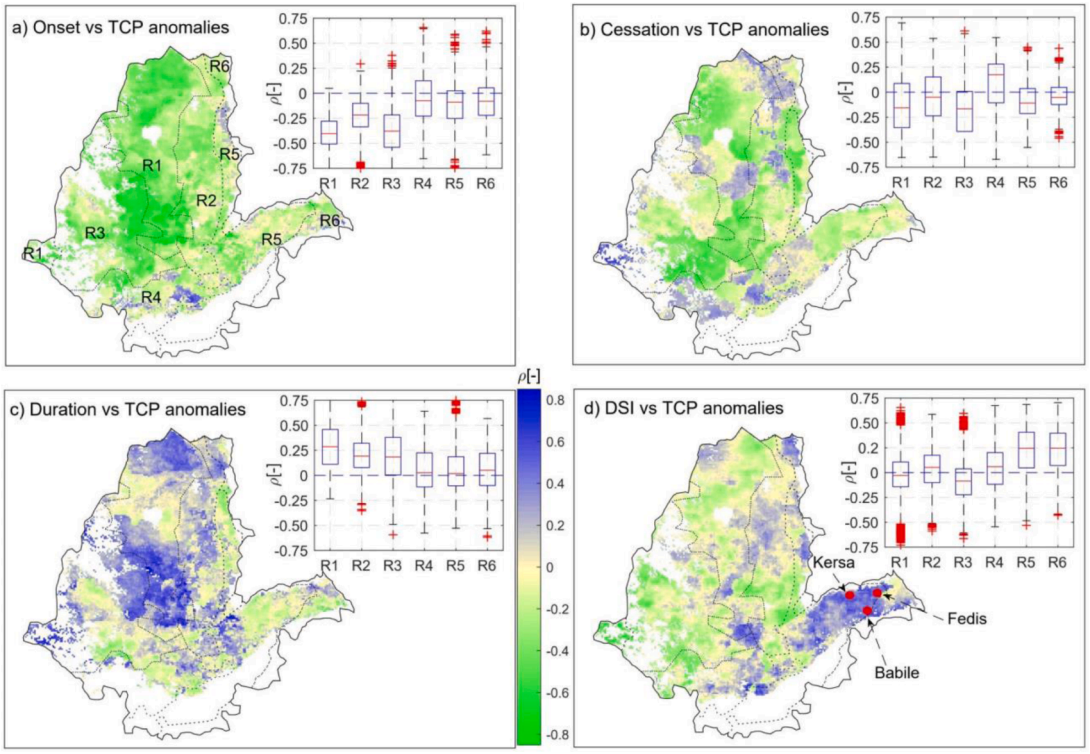

Fig. 10. Pearson correlation coefficient ρ for the relationship between the de-trended total cereal production (TCP) and (a) onset date anomaly (-ve/+ve anomaly corresponds to early/late), (b) cessation date anomaly, (c) rainy season duration anomaly, and (d) DSI anomaly. The red dots in (d) are site locations of a recent study (Tesfaye and Seifu, 2016) where farmers' perception of local climate changes were documented. The boxplots summarize the variability of the correlation in the six rainfall regimes – regime 1 (R1) to regime 6 (R6) (see Fig. 3 for a detailed map). Correlations are computed for the period 1995-2010.

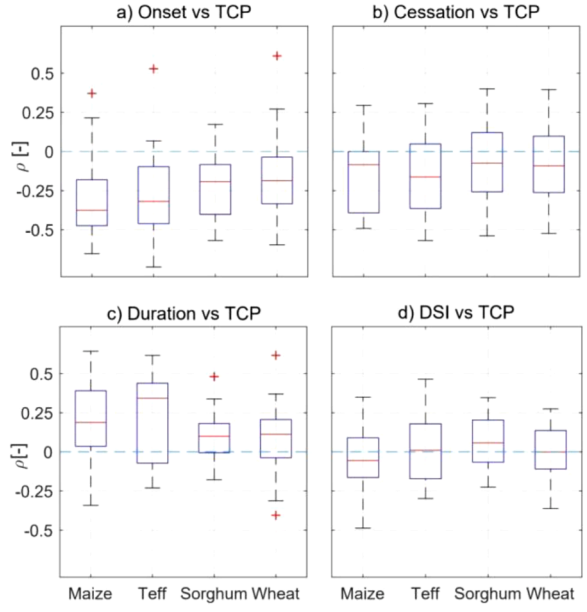

Fig. 11. Pearson correlation (ρ) between the anomaly in production dominated by specific crops and (a) onset anomaly, (b) cessation anomaly, (c) duration anomaly, and (d) DSI anomaly. Boxplots represent the variability between 25 sampled sites in the domain. Correlations are computed for the period 1995-2010.

The strong sensitivity of teff to the onset of the rainy season is linked to its high crop water requirement at the initial stage of growth (shortly after sowing in July/August), with the FAO crop coefficient ($K_{c,\ ini}$) of 0.8 – 1, nearly 3 times that of sorghum and wheat (Araya et al., 2011; Paff and Asseng, 2018). Teff productivity is also affected by water deficit during the grain-filling stage (Mengistu and Mekonnen, 2012), which is 65-72 days after sowing (Araya et al., 2011). The high correlation of maize production with the onset can be explained by the fact that the length of the growing period of maize is about 180 days (Allen et al., 1998) and its sowing in RFA systems starts in April before the onset of rainfall (see Fig. 8a). Hence, the arrival of rainfall in April is critical for the growth of maize during the early stage. Funk et al. (2003) also documented that the April-May rainfall over large parts of Ethiopia determines the subsequent Meher production, thus this can be the case in maize-dominated regions.

The importance of the rainfall onset is not limited to the crop growth period; pre-planting operations like tillage require optimal soil moisture for the soil workability. In the context of the smallholder RFA systems in Ethiopia, where tillage is an intense operation that is carried out using draft animals, the timing of the operation follows the onset or pre-onset of rain showers (Temesgen et al., 2008) when the soil is moist and workable. Therefore, the late-onset of the rainy season delays the tillage operation, which in turn delays the planting activities. The foreseeable way to offset this impact is to improve the tillage power availability, e.g., switching from animal draft power to mechanical (tractor) power when possible.

The impact of the rainy season onset on TCP is highly pronounced in the western and northwestern parts of the RFA area (Fig. 12a) where the rainfall is highly seasonal with a duration ranging from 100 days in the north to 150 days in the lower northwest. The pattern of the impact is similar for the duration but with a lower magnitude (Fig. 12b). The eastward decrease in the magnitude of the changes arises from the fact that crops take advantage of the soil moisture memory from the Belg season in the areas where the rainfall has a bimodal tendency. On average 1.5% reduction in TCP per unit pentad late-onset and a 1.1% reduction in TCP per unit pentad shorter duration of the rainy season is expected across the RFA area during the Meher production, but locally

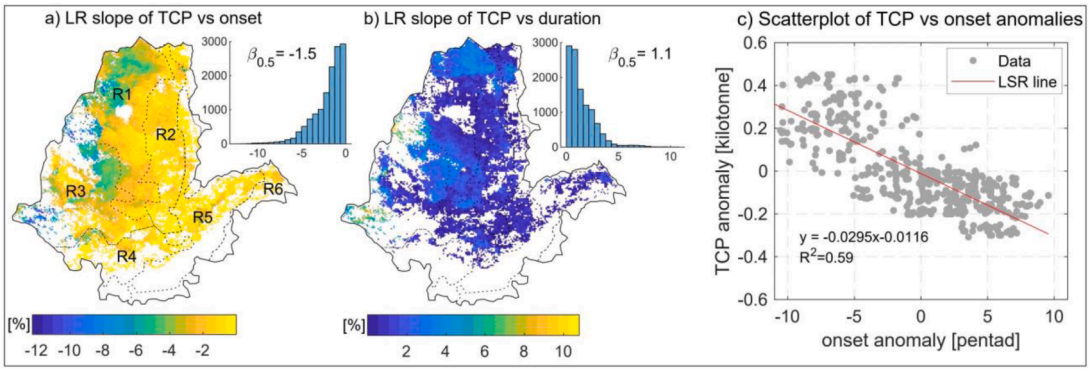

Fig. 12. Changes in the total cereal production in % per pentad of (a) onset anomaly and (b) duration anomaly, computed for the period 1995-2010. The histograms present the distribution of the changes. $\beta_{0.5}$ is the median of the % change in TCP per pentad. (c) Example of linear regression (LR) model performance for TCP vs onset of all grid cell in which TCP is strongly correlated to the rainfall onset (ρ>0.75); the least-squares regression (LSR) line represents an average LR model for these grid cells.

reductions of more than 10% TCP per unit pentad are possible.

The effects of early and late-onset of rainfall tend to differ in terms of variability in the TCP anomaly (see Fig. 12c), which can affect the performance of the linear regression model. This can be linked to the asymmetry of farmers' response to the early and late-onset events. For our purpose, we consider the model performance to be sufficient because it is intended to determine the average rates of changes and spatial patterns of the sensitivity of rainfed crop production to variability and changes in the temporal rainfall attributes in the RFA area. However, we recommend variable transformation in cases of strong nonlinearity, if the use of linear regression models is intended for the prediction of seasonal crop production.

Farmers often respond to a late-onset of the rainy season by adjusting their planting/sowing schedule and thus, planting often takes place after the arrival of the first rainy days (Marteau et al., 2011). The observed reduction in TCP per pentad of late-onset is largely due to the inherent decrease in the total rainfall during the season as a result of the late-onset because the onset of the rainy season and the total rainfall in season are negatively correlated (median ρ = -0.88). This implies that farmers need to implement additional coping strategies, e.g., cultivation of crop varieties that require less water, reducing non-productive rainwater losses (Porkka et al., 2021; Rockström, 2003), such as evaporation (mulching) and runoff outflow (runoff water harvesting), to offset the effect of late-onset of the rainy season on rainfed crop production.

5. Conclusions

The temporal characteristics of rainfall dictate not only the seasonal rainfall amount that is reliably available for crop production but also the timing of the farming activities, including tillage and planting operations, which in turn affect crop production in the RFA system in Ethiopia. In this study, we evaluated the variability and changes in the temporal rainfall attributes – the rainfall seasonality, onset and cessation dates, and duration of the rainy season – and assessed how these may potentially affect cereal crop production.

We found that the northern RFA areas are characterized by high rainfall seasonality, while in the southern RFA areas the rainfall seasonality is less pronounced. The onset of the main rainy season starts in the southern part in early March and advances in the northeast direction until late June or early July, while the cessation dates follow the exact opposite direction starting in late September and ending in the southwest during late October. The northeastern semi-arid region is climatologically unstable, as it undergoes substantial changes and interannual variability in rainfall seasonality, timing and duration of the rainy season, and this is predominantly related to the frequent failure of Belg (February - May) rainfall.

Cereal production during the Meher season is highly correlated to the onset and length of the rainy season in regions where the rainfall seasonality is high. The highest (and negative) correlation between onset and total cereal production is observed in maize (ρ=-0.37) and teff (ρ=-0.32) dominated areas. The effects of late-onset and shorter duration of the rainy season on crop production are more pronounced in the western part of the RFA areas where the rainfall has a unimodal pattern and the effects are less evident in the eastern parts where the rainfall pattern is bimodal. On average, a late-onset of the rainy season leads to 1.5% of rainfed cereal crop production loss per pentad, while a shorter rainy season leads to 1.1% of production loss per pentad. The cessation of the rainy season has less effect on crop production. In regions with a bimodal rainfall regime, the Meher cereal production is positively correlated to rainfall seasonality. This is particularly the case in the eastern highland regions where the limited annual rainfall is distributed over two shorter and agriculturally less relevant seasons.

With this analysis, we demonstrate that temporal rainfall attributes in relation to rainfed agriculture can provide useful information for the prediction of seasonal crop production. We expect that such information can be useful for developing early warning systems, RFA system vulnerability assessment, and for climate adaptation planning for sustainable food production in Ethiopia. The methods used in this study can be extended to other regions including other East African countries to understand the response of crop production to the temporal properties of rainfall. However, we advise against direct extrapolation and scaling of the findings of this study for a different region because crop productivity differs between regions depending on the existing agrometeorological services, farming technologies and other factors that can support farmers' decision and actions to respond to weather and climate variabilities.

Declaration of Competing Interest

The authors declare that they have no known competing financial interests or personal relationships that could have appeared to influence the work reported in this paper.

Acknowledgment

This research is funded by the Engineering for Development E4D Doctoral Scholarship Program of ETH for Development (ETH4D), ETH Zurich, as part of the research project 'Rainfed agriculture in Ethiopia: climate vulnerability and adaptation'.

References

Alhamshry, A., Fenta, A.A., Yasuda, H., Kimura, R., Shimizu, K., 2020. Seasonal rainfall variability in Ethiopia and its long-term link to global sea surface temperatures. Water (Switzerland) 12, 1–19. https://doi.org/10.3390/w12010055.

Allen, R.G., Pereira, L.S., Raes, D., Smith, M., 1998. Crop Evapotranspiration, Irrigation and Drainage Paper No. 56. Rome.

Araya, A., Stroosnijder, L., 2011. Assessing drought risk and irrigation need in northern Ethiopia. Agric. For. Meteorol. 151, 425–436. https://doi.org/10.1016/j.agrformet.2010.11.014.

Araya, A., Stroosnijder, L., Girmay, G., Keesstra, S.D., 2011. Crop coefficient, yield response to water stress and water productivity of teff (Eragrostis tef (Zucc.). Agric. Water Manag. 98, 775–783. doi:10.1016/j.agwat.2010.12.001.

Asrat, P., Simane, B., 2018. Farmers' perception of climate change and adaptation strategies in the Dabus watershed, North-West Ethiopia. Ecol. Process. 7 https://doi.org/10.1186/s13717-018-0118-8.

Ayanlade, A., Radeny, M., Morton, J.F., Muchaba, T., 2018. Rainfall variability and drought characteristics in two agro-climatic zones: an assessment of climate change challenges in Africa. Sci. Total Environ. 630, 728–737. https://doi.org/10.1016/j.scitotenv.2018.02.196.

Bayissa, Y., Tadesse, T., Demisse, G., Shiferaw, A., 2017. Evaluation of satellite-based rainfall estimates and application to monitor meteorological drought for the Upper Blue Nile Basin, Ethiopia. Remote Sens. 9, 1–17. https://doi.org/10.3390/rs9070669.

Berhane, F., Zaitchik, B., 2014. Modulation of daily precipitation over East Africa by the Madden-Julian oscillation. J. Clim. 27, 6016–6034. https://doi.org/10.1175/JCLI-D-13-00693.1.

Buchhorn, M., Smets, B., Bertels, L., De Roo, B., Lesiv, M., Tsendbazar, Nandin-Erdene Tarko, A, 2020. Copernicus global land operations "Vegetation and Energy" "CGLOPS-1.". Copernicus Glob. L. Oper. 1–93. https://doi.org/10.5281/zenodo.3938963.PU.

Camberlin, P., 1997. Rainfall anomalies in the source region of the Nile and their connection with the Indian summer monsoon. J. Clim. 10, 1380–1392. https://doi.org/10.1175/1520-0442(1997)010<1380:RAITSR>2.0.CO;2.

Cheung, W.H., Senay, G.B., Singh, A., 2008. Trends and spatial distribution of annual and seasonal rainfall in Ethiopia. Int. J. Climatol. 28, 1723–1734. https://doi.org/10.1002/joc.

Cleveland, W.S., 1979. Robust locally weighted regression and smoothing scatterplots. J. Am. Stat. Assoc. 74, 829–836. https://doi.org/10.1080/01621459.1979.10481038.

Borchert, R., 1998. Responses of tropical trees to rainfall seasonality and its long-term changes,in: Potential Impacts of Climate Change on Tropical Forest Ecosystems. Springer, pp. 381–393.

Cover, T.M., Thomas, J.A., 2005. Elements of information theory, Elements of information theory. doi:10.1002/047174882X.

CSA, 2016. Agricultural sample Survery 2015/16 (2008 E.C): report on Area, production and farm management practice of Belg season crops for private peasant holdings. Statistical Bulletin.

CSA, 2010. Area and production of crops, Agricultural Sample Survey. Addis Ababa.

CSA, 2007. Summary and statistical report of the 2007 population and housing census. Addis Ababa.

Degefu, M.A., Rowell, D.P., Bewket, W., 2017. Teleconnections between Ethiopian rainfall variability and global SSTs: observations and methods for model evaluation. Meteorol. Atmos. Phys. 129, 173–186. https://doi.org/10.1007/s00703-016-0466-9.

Dinku, T., Chidzambwa, S., Ceccato, P., Connor, S.J., Ropelewski, C.F., 2008. Validation of high-resolution satellite rainfall products over complex terrain. Int. J. Remote Sens. 29, 4097–4110. https://doi.org/10.1080/01431160701772526.

Dinku, T., Funk, C., Peterson, P., Maidment, R., Tadesse, T., Gadain, H., Ceccato, P., 2018. Validation of the CHIRPS satellite rainfall estimates over eastern. Africa. Q. J. R. Meteorol. Soc. 144, 292–312. https://doi.org/10.1002/qj.3244.

Diro, G.T., Grimes, D.I.F., Black, E., 2011a. Teleconnections between Ethiopian summer rainfall and sea surface temperature: part I-observation and modelling. Clim. Dyn. 37, 103–119. https://doi.org/10.1007/s00382-010-0837-8.

Diro, G.T., Grimes, D.I.F., Black, E., 2011b. Teleconnections between Ethiopian summer rainfall and sea surface temperature: part II. Seasonal forecasting. Clim. Dyn. 37, 121–131. https://doi.org/10.1007/s00382-010-0896-x.

Dodd, D.E.S., Jolliffe, I.T., 2001. Early detection of the start of the wet season in semiarid tropical climates of Western Africa. Int. J. Climatol. 21, 1251–1262. https://doi.org/10.1002/joc.640.

Dubois, N., Oppo, D.W., Galy, V.V., Mohtadi, M., Van Der Kaars, S., Tierney, J.E., Rosenthal, Y., Eglinton, T.I., Lückge, A., Linsley, B.K., 2014. Indonesian vegetation response to changes in rainfall seasonality over the past 25,000 years. Nat. Geosci. 7, 513–517. https://doi.org/10.1038/ngeo2182.

Dunning, C.M., Black, E., Allan, R.P., 2018. Later wet seasons with more intense rainfall over Africa under future climate change. J. Clim. 31, 9719–9738. https://doi.org/10.1175/JCLI-D-18-0102.1.

Dunning, C.M., Black, E.C.L., Allan, R.P., 2016. The onset and cessation of seasonal rainfall over Africa. J. Geophys. Res. 121, 11405–11424. https://doi.org/10.1002/2016JD025428.

Falkenmark, M., 2006. The new blue and green water paradigm: breaking new ground for water resources planning and management 132, 129–132. doi:10.1061/(ASCE)0733-9496(2006)132.

FAO, 1986. Irrigation Water Management: irrigation Water Needs [WWW Document]. URL http://www.fao.org/3/S2022E/s2022e06.htm#2.1 major climatic zones (accessed 2.13.21).

FAOSTAT, 2018. Land use indicators [WWW Document]. URL http://www.fao.org/faostat/en/#data/EL (accessed 10.21.20).

Feng, X., Porporato, A., Rodriguez-Iturbe, I., 2013. Changes in rainfall seasonality in the tropics. Nat. Clim. Chang. 3 https://doi.org/10.1038/NCLIMATE1907.

Funk, C., Asfaw, A., Phil, S., Gabriel, S., Jim, R., 2003. Estimating Meher Crop Production Using Rainfall in the ' Long Cycle ' Statistical Estimates of Meher Yields Based on April-May Rainfall Totals. Addis Ababa.

Funk, C., Peterson, P., Landsfeld, M., Pedreros, D., Verdin, J., Shukla, S., Husak, G., Rowland, J., Harrison, L., Hoell, A., Michaelsen, J., 2015. The climate hazards infrared precipitation with stations-a new environmental record for monitoring extremes. Nat. Sci. Data 2. https://doi.org/10.1038/sdata.2015.66.

Funk, C., Senay, G., Asfaw, A., Verdin, J., Rowland, J., Michaelson, J., Eilerts, G., Korecha, D., Choularton, R., 2005. Recent drought tendencies in Ethiopia and equatorial-subtropical eastern Africa. Famine Early Warning System Network. U.S. Agency Int. Dev. 11.

Gaetani, M., Janicot, S., Vrac, M., Famien, A.M., Sultan, B., 2020. Robust assessment of the time of emergence of precipitation change in West Africa. Sci. Rep. 10, 1–10. https://doi.org/10.1038/s41598-020-63782-2.

Gebeyehu, M.G., 2016. The impact of technology adoption on agricultural productivity and production risk in Ethiopia: evidence from rural Amhara household survey. OALib 03, 1–14. https://doi.org/10.4236/oalib.1102369.

Gebrechorkos, S.H., Hülsmann, S., Bernhofer, C., 2018. Evaluation of multiple climate data sources for managing environmental resources in East Africa. Hydrol. Earth Syst. Sci 22, 4547–4564. https://doi.org/10.5194/hess-22-4547-2018.

Gebremicael, T.G., Mohamed, Y.A., Zaag, P.van der, Gebremedhin, A., Gebremeskel, G., Yazew, E., Kifle, M., 2019. Evaluation of multiple satellite rainfall products over the rugged topography of the Tekeze-Atbara basin in Ethiopia. Int. J. Remote Sens. 40, 4326–4345. https://doi.org/10.1080/01431161.2018.1562585.

Gissila, T., Black, E., Grimes, D.I.F., Slingo, J.M., 2004. Seasonal forecasting of the Ethiopian summer rains. Int. J. Climatol. 24, 1345–1358. https://doi.org/10.1002/joc.1078.

Gleixner, S., Keenlyside, N., Viste, E., Korecha, D., 2017. The El Niño effect on Ethiopian summer rainfall. Clim. Dyn. 49, 1865–1883. https://doi.org/10.1007/s00382-016-3421-z.

González, M., Vera, C.S., Liebmann, B., Marengo, J.A., Kousky, V., Allured, D., 2007. The nature of the rainfall onset over central South America. Atmosfera 20, 377–394.

Guan, K., Sultan, B., Biasutti, M., Baron, C., Lobell, D.B., 2015. What aspects of future rainfall changes matter for crop yields in West Africa? Geophys. Res. Lett. 42, 8001–8010. https://doi.org/10.1002/2015GL063877.

Guhathakurta, P., Saji, E., 2013. Detecting changes in rainfall pattern and seasonality index vis-à-vis increasing water scarcity in Maharashtra. J. Earth Syst. Sci. 122, 639–649. https://doi.org/10.1007/s12040-013-0294-y.

Guido, Z., Zimmer, A., Lopus, S., Hannah, C., Gower, D., Waldman, K., Krell, N., Sheffield, J., Caylor, K., Evans, T., 2020. Farmer forecasts: impacts of seasonal rainfall expectations on agricultural decision-making in Sub-Saharan Africa. Clim. Risk Manag. 30, 100247. doi:10.1016/j.crm.2020.100247.

Habtemariam, L.T., Gandorfer, M., Kassa, G.A., Heissenhuber, A., 2016. Factors influencing smallholder Farmers' climate change perceptions: a study from farmers in Ethiopia. Environ. Manage. 58, 343–358. https://doi.org/10.1007/s00267-016-0708-0.

Hampf, A.C., Stella, T., Berg-Mohnicke, M., Kawohl, T., Kilian, M., Nendel, C., 2020. Future yields of double-cropping systems in the Southern Amazon, Brazil, under climate change and technological development. Agric. Syst. 177 https://doi.org/10.1016/j.agsy.2019.102707.

Hao, F., Chen, S., Ouyang, W., Shan, Y., Qi, S., 2013. Temporal rainfall patterns with water partitioning impacts on maize yield in a freeze – thaw zone. J. Hydrol. 486, 412–419. https://doi.org/10.1016/j.jhydrol.2013.02.008.

Hills, R.C., 1979. The structure of the inter-tropical convergence zone in equatorial Africa and its relationship to east African rainfall. Trans. Inst. Br. Geogr. 4, 329–352. https://doi.org/10.2307/622055.

Hundera, H., Mpandeli, S., Bantider, A., 2019. Smallholder farmers' awareness and perceptions of climate change in Adama district, central rift valley of Ethiopia. Weather Clim. Extrem. 26, 100230 https://doi.org/10.1016/j.wace.2019.100230.

IFPRI, CSA, 2006. Atlas of the Ethiopian Rural Economy. Atlas of the Ethiopian Rural Economy. International Food Policy Research Institute, Washinton DC. https://doi.org/10.2499/0896291545.

Jiang, Y., Zhou, L., Tucker, C.J., Raghavendra, A., Hua, W., Liu, Y.Y., Joiner, J., 2019. Widespread increase of boreal summer dry season length over the Congo rainforest. Nat. Clim. Chang. 9, 617–622. https://doi.org/10.1038/s41558-019-0512-y.

Kahsay, H.T., Guta, D.D., Birhanu, B.S., Gidey, T.G., Routray, J.K., 2019. Farmers' perceptions of climate change trends and adaptation strategies in semiarid highlands of eastern tigray, Northern Ethiopia. Adv. Meteorol. https://doi.org/10.1155/2019/3849210, 2019.

Kassawmar, T., Zeleke, G., Bantider, A., Gessesse, G.D., Abebe, S., Abraha, L., Tadesse, M., 2019. State of cropland availability in rainfed farming systems in Ethiopia: alternative pathways to address landlessness and food insecurity. In: Ethiopia: Social and Political Issues, in: Ethiopia: Social and Political Issues. NOVA, pp. 228–260.

Kassawmar, T., Zeleke, G., Bantider, A., Gessesse, G.D., Abraha, L., 2018. A synoptic land change assessment of Ethiopia's Rainfed Agricultural Area for evidence-based agricultural ecosystem management. Heliyon 4, 914. https://doi.org/10.1016/j.heliyon.2018.e00914.

Kebede, A., Diekkrüger, B., Edossa, D.C., 2017. Dry spell, onset and cessation of the wet season rainfall in the Upper Baro-Akobo Basin. Ethiopia. Theor. Appl. Climatol. 129, 849–858. https://doi.org/10.1007/s00704-016-1813-y.

Kendall, M.G., 1975. Ranked Correlation Methods, 4th ed. Behavior Research Methods, Instruments, & Computers, Charles Griffin, London. https://doi.org/10.3758/bf03202470.
Korecha, D., Barnston, A.G., 2007. Predictability of June-september rainfall in Ethiopia. Mon. Weather Rev. 135, 628–650. https://doi.org/10.1175/MWR3304.1.
Kukal, M.S., Irmak, S., 2018. Climate-driven crop yield and yield variability and climate change Impacts on the U.S. Great Plains Agricultural Production. Nat. Sci. Rep. 8, 1–18. https://doi.org/10.1038/s41598-018-21848-2.
Liebmann, B., Bladé, I., Kiladis, G.N., Carvalho, L.M.V., Senay, G.B., Allured, D., Leroux, S., Funk, C., 2012. Seasonality of African precipitation from 1996 to 2009. J. Clim. 25, 4304–4322. https://doi.org/10.1175/JCLI-D-11-00157.1.
Liebmann, B., Marengo, J.A., 2001. Interannual variability of the rainy season and rainfall in the Brazilian Amazon Basin. J. Clim. 14, 4308–4318. https://doi.org/10.1175/1520-0442(2001)014<4308:IVOTRS>2.0.CO;2.
MacLeod, D., 2018. Seasonal predictability of onset and cessation of the east African rains. Weather Clim. Extrem. 21, 27–35. https://doi.org/10.1016/j.wace.2018.05.003.
Mann, H.B., 1945. H.B. Mann Nonparametric tests against trend Econometrica. Econometrica 245–259.
Marengo, J.A., Liebmann, B., Kousky, V.E., Filizola, N.P., Wainer, I.C., 2001. Onset and end of the rainy season in the Brazilian Amazon Basin. J. Clim. 14, 833–852. https://doi.org/10.1175/1520-0442(2001)014<0833:OAEOTR>2.0.CO;2.
Marteau, R., Moron, V., Philippon, N., 2009. Spatial coherence of Monsoon onset over Western and Central Sahel (1950-2000). J. Clim. 22, 1313–1324. https://doi.org/10.1175/2008JCLI2383.1.
Marteau, R., Sultan, B., Moron, V., Alhassane, A., Baron, C., Traoré, S.B., 2011. The onset of the rainy season and farmers' sowing strategy for pearl millet cultivation in Southwest Niger. Agric. For. Meteorol. 151, 1356–1369. https://doi.org/10.1016/j.agrformet.2011.05.018.
Mengistu, D.K., Mekonnen, L.S., 2012. Integrated Agronomic Crop Managements to Improve Tef Productivity Under Terminal Drought, in: Rahman, P.I.M.M. (Ed.), Water Stress. pp. 235–254.
Mugalavai, E.M., Kipkorir, E.C., Raes, D., Rao, M.S., 2008. Analysis of rainfall onset, cessation and length of growing season for western Kenya. Agric. For. Meteorol. 148, 1123–1135. https://doi.org/10.1016/j.agrformet.2008.02.013.
Musie, M., Sen, S., Srivastava, P., 2019. Comparison and evaluation of gridded precipitation datasets for streamflow simulation in data scarce watersheds of Ethiopia. J. Hydrol. 579, 124168 https://doi.org/10.1016/j.jhydrol.2019.124168.
Mutsaers, H.J.W., 1979. An agricultural analysis of rainfall reliability for Cameroon. Netherlands J. Agric. Sci. 27, 67–78. https://doi.org/10.18174/njas.v27i1.17072.
Omotosho, J.B., Balogun, A.A., Ogunjobi, K., 2000. Predicting monthly and seasonal rainfall, onset and cessation of the rainy season in West Africa using only surface data. Int. J. Climatol. 20, 865–880. https://doi.org/10.1002/1097-0088(20000630)20:8<865:AID-JOC505>3.0.CO;2-R.
Psajiaff, K., Asseng, S., 2018. A review of tef physiology for developing a tef crop model. Eur. J. Agron. 94, 54–66. https://doi.org/10.1016/j.eja.2018.01.008.
Pascale, S., Lucarini, V., Feng, X., Porporato, A., ul Hasson, S., 2016. Projected changes of rainfall seasonality and dry spells in a high greenhouse gas emissions scenario. Clim. Dyn. 46, 1331–1350. https://doi.org/10.1007/s00382-015-2648-4.
Philip, S., Kew, S.F., van Oldenborgh, G.J., Otto, F., O'Keefe, S., Haustein, K., King, A., Zegeye, A., Eshetu, Z., Hailemariam, K., Singh, R., Jjemba, E., Funk, C., Cullen, H., 2018. Attribution analysis of the Ethiopian drought of 2015. J. Clim. 31, 2465–2486. https://doi.org/10.1175/JCLI-D-17-0274.1.
Porkka, M., Wang-Erlandsson, L., Destouni, G., Ekman, A.M.L., Rockström, J., Gordon, L. J., 2021. Is wetter better? Exploring agriculturally-relevant rainfall characteristics over four decades in the Sahel. Environ. Res. Lett. 16 https://doi.org/10.1088/1748-9326/abdd57.
Potter, N.J., Zhang, L., Milly, P.C.D., McMahon, T.A., Jakeman, A.J., 2005. Effects of rainfall seasonality and soil moisture capacity on mean annual water balance for Australian catchments. Water Resour. Res. 41, 1–11. https://doi.org/10.1029/2004WR003697.
Radeny, M., Desalegn, A., Mubiru, D., Kyazze, F., Mahoo, H., Recha, J., Kimeli, P., Solomon, D., 2019. Indigenous knowledge for seasonal weather and climate forecasting across East Africa. Clim. Change 156, 509–526. https://doi.org/10.1007/s10584-019-02476-9.
Raes, D., Sithole, A., Makarau, A., Milford, J., 2004. Evaluation of first planting dates recommended by criteria currently used in Zimbabwe. Agric. For. Meteorol. 125, 177–185. https://doi.org/10.1016/j.agrformet.2004.05.001.
Rockström, J., 2003. Water for food and nature in drought-prone tropics: vapour shift in rain-fed agriculture. Philos. Trans. R. Soc. B Biol. Sci. 358, 1997–2009. https://doi.org/10.1098/rstb.2003.1400.
Rohr, T., Manzoni, S., Feng, X., Menezes, R.S.C., Porporato, A., 2013. Effect of rainfall seasonality on carbon storage in tropical dry ecosystems. J. Geophys. Res. Biogeosciences 118, 1156–1167. https://doi.org/10.1002/jgrg.20091.
Sadiq, A.A., 2020. An estimation of rainfall seasonality index of Yola south LGA and its effects on agriculture and environment. African J. Environ. Nat. Sci. Res. 3, 57–72.
Saha, S., Moorthi, S., Pan, H.L., Wu, X., Wang, Jiande, Nadiga, S., Tripp, P., Kistler, R., Woollen, J., Behringer, D., Liu, H., Stokes, D., Grumbine, R., Gayno, G., Wang, Jun, Hou, Y.T., Chuang, H.Y., Juang, H.M.H., Sela, J., Iredell, M., Treadon, R., Kleist, D., Van Delst, P., Keyser, D., Derber, J., Ek, M., Meng, J., Wei, H., Yang, R., Lord, S., Van Den Dool, H., Kumar, A., Wang, W., Long, C., Chelliah, M., Xue, Y., Huang, B., Schemm, J.K., Ebisuzaki, W., Lin, R., Xie, P., Chen, M., Zhou, S., Higgins, W., Zou, C. Z., Liu, Q., Chen, Y., Han, Y., Cucurull, L., Reynolds, R.W., Rutledge, G., Goldberg, M., 2010. The NCEP climate forecast system reanalysis. Bull. Am. Meteorol. Soc. 91, 1015–1057. https://doi.org/10.1175/2010BAMS3001.1.
Segele, Z.T., Lamb, P.J., 2005. Characterization and variability of Kiremt rainy season over Ethiopia. Meteorol. Atmos. Phys. 89, 153–180. https://doi.org/10.1007/s00703-005-0127-x.
Segele, Z.T., Lamb, P.J., Leslie, L.M., 2009a. Seasonal-to-interannual variability of Ethiopia/horn of Africa monsoon. Part I: associations of wavelet-filtered large-scale atmospheric circulation and global sea surface temperature. J. Clim. 22, 3396–3421. https://doi.org/10.1175/2008JCLI2859.1.
Segele, Z.T., Lamb, P.J., Leslie, L.M., 2009b. Large-scale atmospheric circulation and global sea surface temperature associations with Horn of Africa June–September rainfall. Int. J. Climatol. 29, 1075–1100. https://doi.org/10.1002/joc.1751.
Segele, Z.T., Richman, M.B., Leslie, L.M., Lamb, P.J., 2015. Seasonal-to-interannual variability of ethiopia/horn of Africa monsoon. Part II: statistical multimodel ensemble rainfall predictions. J. Clim. 28, 3511–3536. https://doi.org/10.1175/JCLI-D-14-00476.1.
Seleshi, Y., Camberlin, P., 2006. Recent changes in dry spell and extreme rainfall events in Ethiopia. Theor. Appl. Climatol. 83, 181–191. https://doi.org/10.1007/s00704-005-0134-3.
Seleshi, Y., Zanke, U., 2004. Recent changes in rainfall and rainy days in Ethiopia. Int. J. Climatol. 24, 973–983. https://doi.org/10.1002/joc.1052.
Sen, P.K., 1968. Estimates of the regression coefficient based on Kendall's. Tau. J. Am. Stat. Assoc. 63, 1379–1389. https://doi.org/10.1080/01621459.1968.10480934.
Shanko, D., Camberlin, P., 1998. The effects of the southwest Indian ocean tropical cyclones on Ethiopian drought. Int. J. Climatol. 18, 1373–1388. https://doi.org/10.1002/(SICI)1097-0088(1998100)18:12<1373:AID-JOC313>3.0.CO;2-K.
Shikur, Z.H., 2020. Agricultural policies, agricultural production and rural households' welfare in Ethiopia. J. Econ. Struct. 9 https://doi.org/10.1186/s40008-020-00228-y.
Souza, R., Feng, X., Antonino, A., Montenegro, S., Souza, E., Porporato, A., 2016. Vegetation response to rainfall seasonality and interannual variability in tropical dry forests. Hydrol. Process. 30, 3583–3595. https://doi.org/10.1002/hyp.10953.
Suepa, T., Qi, J., Lawawirojwong, S., Messina, J.P., 2016. Understanding spatio-temporal variation of vegetation phenology and rainfall seasonality in the monsoon Southeast Asia. Environ. Res. 147, 621–629. https://doi.org/10.1016/j.envres.2016.02.005.
Taffesse, A.S., Dorosh, P., Gemessa, S.A., 2012. Crop production in Ethiopia: regional patterns and trends. Summary of report Ethiopian strategy support program (ESSP II), Research Note 11, IFPRI and EDRI, Addis Ababa, Ethiopia (No. 16).
Taye, M.T., Dyer, E., Charles, K.J., Hirons, L.C., 2021. Potential predictability of the Ethiopian summer rains: understanding local variations and their implications for water management decisions. Sci. Total Environ. 755, 142604 https://doi.org/10.1016/j.scitotenv.2020.142604.
Temam, D., Uddameri, V., Mohammadi, G., Hernandez, E.A., Ekwaro-Osire, S., 2019. Long-term drought trends in Ethiopia with implications for dryland agriculture. Water (Switzerland) 11, 1–22. https://doi.org/10.3390/w11122571.
Temesgen, M., Rockstrom, J., Savenije, H.H.G., Hoogmoed, W.B., Alemu, D., 2008. Determinants of tillage frequency among smallholder farmers in two semi-arid areas in Ethiopia. Phys. Chem. Earth 33, 183–191. https://doi.org/10.1016/j.pce.2007.04.012.
Tesfahunegn, G.B., Mekonen, K., Tekle, A., 2016. Farmers' perception on causes, indicators and determinants of climate change in northern Ethiopia: implication for developing adaptation strategies. Appl. Geogr. 73, 1–12. https://doi.org/10.1016/j.apgeog.2016.05.009.
Tesfaye, W., Seifu, L., 2016. Climate change perception and choice of adaptation strategies: empirical evidence from smallholder farmers in east Ethiopia. Int. J. Clim. Chang. Strateg. Manag. 8, 253–270. https://doi.org/10.1108/IJCCSM-01-2014-0017.
Torres, M., Howitt, R., Rodrigues, L., 2019. Analyzing rainfall effects on agricultural income: why timing matters. EconomiA 20, 1–14. https://doi.org/10.1016/j.econ.2019.03.006.
Victor, U.S., Srivastava, N.N., Subba Rao, A.V.M., Ramana Rao, B.V., 1996. Managing the impact of seasonal rainfall variability through response farming at a semi-arid tropical location. Curr. Sci. 71, 392–397.
Viste, E., Korecha, D., Sorteberg, A., 2013. Recent drought and precipitation tendencies in Ethiopia. Theor. Appl. Climatol. 112, 535–551. https://doi.org/10.1007/s00704-012-0746-3.
Viste, E., Sorteberg, A., 2013. Moisture transport into the Ethiopian highlands. Int. J. Climatol. 33, 249–263. https://doi.org/10.1002/joc.3409.
Walsh, R.P.D., Lawler, D.M., 1981. Rainfall Seasonality: description, Spatial Patterns and Change Through Time. Weather 36, 201–208. https://doi.org/10.1002/j.1477-8696.1981.tb05400.x.
Wani, S.P., Rockström, J., Oweis, T., 2009. Rain-Fed Agriculture: Unlocking the Potential. CAB International. CABI, London.
Williams, A.P., Funk, C., Michaelsen, J., Rauscher, S.A., Robertson, I., Wils, T.H.G., Koprowski, M., Eshetu, Z., Loader, N.J., 2012. Recent summer precipitation trends in the Greater Horn of Africa and the emerging role of Indian Ocean sea surface temperature. Clim. Dyn. 39, 2307–2328. https://doi.org/10.1007/s00382-011-1222-y.
Yengoh, G.T., Armah, F.A., Onumah, E.E., Odoi, J.O., 2010. Trends in agriculturally-relevant rainfall characteristics for small-scale agriculture in Northern Ghana. J. Agric. Sci. 2, 3–16. https://doi.org/10.5539/jas.v2n3p3.
Zhang, W., Brandt, M., Tong, X., Tian, Q., Fensholt, R., 2018. Impacts of the seasonal distribution of rainfall on vegetation productivity across the Sahel. Biogeosciences 15, 319–330. https://doi.org/10.5194/bg-15-319-2018.